Characteristics of vertical velocities estimated from drop size and fall velocity spectra of a Parsivel disdrometer

Dong-Kyun Kim and Chang-Keun Song

School of Urban and Environmental Engineering,
Ulsan National Institute of Science and Technology, Ulsan, Korea

Submitted to Atmospheric Measurement Techniques

21 June 2018

Corresponding Author: Prof. Chang-Keun Song, School of Urban and Environmental Engineering, Ulsan National Institute of Science and Technology, Ulsan, Korea, Email:cksong@unist.ac.kr

Abstract

Vertical air velocities were estimated from drop size and fall velocity spectra observed by Parsivel disdrometers during intensive field observations from 13 June to 3 August 2016 around Mt. Jiri (1915 m above sea level) in the southern Korean Peninsula. Rainfall and wind velocity data measured by Parsivel disdrometers and ultrasonic anemometers, respectively, were analyzed for an orographic rainfall event associated with a stationary front over Mt. Jiri on 1 July 2016. In this study, a new technique was developed to estimate vertical air velocities from drop size and fall velocity spectra measured by the Parsivel disdrometers and investigate characteristics of up-/downdrafts and related microphysics in the windward and leeward side of the mountain.

To validate results from this technique, vertical air velocities between the Parsivel disdrometers and anemometers were compared at different locations and were shown in quite good agreement each other. It was shown that upward motions were relatively more dominant in the windward side and even during periods of heavy rainfall. On the contrast, downward motions were more dominant in the leeward side during nearly the same periods of heavy rainfall. Occurrences of upward and downward motion were digitized as percentage values as they are divided by a total count of occurrences during the entire period. In the windward (leeward) side, the percentages of upward (downward) motion were much larger than those of downward (upward) motion. The mean rainfall intensity in the leeward side was stronger than in the windward side, suggesting that most of the rainfall in the leeward side was relatively more affected by the downward motions.

Key words: vertical air velocity, drop size spectra, DSD parameter, Parsivel disdrometer

1. Introduction

Drop size distribution (DSD) and related rain parameters from surface disdrometer measurements or indirectly retrieved from remote sensing measurements such as radars, wind profilers, or satellites provide key information for a better understanding of rain microphysics that accounts for drop growth and precipitation processes. Nevertheless, DSD uncertainties always exist as its retrieval is vulnerable to various factors such as measurement errors, sampling difference in volume and height, strong winds, up-/downdrafts, turbulence, and so on as have been reported in many previous studies (Jameson and Kostinski 1998; Cao et al., 2008; Tokay et al., 2009; Thurai et al., 2012). Thus a validation of such retrieved DSDs by comparing with those from surface disdrometers is not straightforward (Williams et al. 2000) due to their different environment although minimizing a sampling difference as much as possible is needed. Even if DSDs are accurately obtained, their characteristics, particularly between convective and stratiform rain, can vary largely from small areas in short-time scale to climatic regimes in long-term.

Ground-based classifications of convective, mixed, or stratiform rain type have been performed in various ways such as characteristics in integral DSD parameters (i.e., rain rate, mean drop diameter, etc), bright band signature, vertical gradients in Doppler velocity and reflectivity, vertical draft magnitude, and so on (Atlas et al., 2000; Cifelli et al., 2000; Thompson et al., 2015; Tokay and Short 1996; Tokay et al., 1996, 1999; Thurai et al., 2016; Williams et al., 1995). Tokay et al. (1999) classified rainfall types from collocated disdrometer and 915 MHz profiler observations in tropical rain events and indicated that compared to profiler classifications that utilize vertical gradients in Doppler velocity, a disdrometer is relatively more feasible to misclassify stratiform rain as convective or vice versa due to time-height ambiguity mostly associated with advection of drops while falling to the ground.

In measuring and validating surface DSDs, there is no such handy, transportable, and low-cost instrument like disdrometer that has long been used as a ground truth although it has inherent problems mentioned above as exposed to all different environments. Parsivel disdrometer (hereafter Parsivel) is one of disdrometers widely used for DSD studies over the world. As deduced from its name, par-si-vel (particle size and velocity), this disdrometer measures sizes, fall velocities, and number counts of liquid and ice particles falling into 32 (size) x 32 (fall velocity) bins. Parsivel has been used at observatories or in numerous field experiments to examine and validate microphysical properties by comparing DSDs and integral DSD parameters with those from other type disdrometer, 2-Dimentional Video Disdrometer (2DVD), wind profiler, and radar observations for various events of precipitation (Jaffrain and Berne 2011; Kim et al., 2016; Thurai et al., 2011, 2016; Tokay et al., 2013).

A Parsivel-measured fall velocity of a raindrop is the sum of a raindrop terminal fall speed (in stagnant air) and vertical air motion. Thus when there are updrafts or downdrafts, the Parsivel-measured fall velocity is deviated from the terminal fall speed even if drop sizes are identical. On top of this, strong horizontal winds, vertical shear, or turbulence can disperse the distribution of drop size and fall velocity, leading to a change (or bias) in the Parsivel-measured fall velocity averaged over the distribution. Consequently, all these factors would affect DSD integral parameters such as rain rate although the effects of the factors on DSD are complicated and hardly discriminated (Niu et al., 2010). Ulbrich (1992) examined errors in rain rate that result from inaccuracies in fall speeds of raindrops (i.e., inaccurate estimation of vertical air motion) and indicated that updraft will result in larger rain rate at a given reflectivity than when there are no vertical winds. Niu et al. (2010) investigated differences in distributions of drop sizes and fall velocities between convective and stratiform rain and ascribed different deviations in Parsivel-measured fall velocities between small and

116 large drops to vertical air motion and turbulence. Parsivel is prone to measurement errors
117 particularly when there are strong winds and turbulence, leading to discrepancies in
118 comparison with other measurements in the same locations. Friedrich et al. (2013)
119 investigated the influence of strong winds on particle size distributions measured by Parsivel
120 disdrometers deployed in Hurricane Ike 2008 and convective storms and noted that
121 misclassification can occur by particles not falling perpendicular to the sampling area at high
122 wind speed and/or heavy rainfall. Tokay et al. (2009, 2014) indicated that the old version of
123 Parsivel tends to underestimate the number of small drops and overestimate drop size larger
124 than 2.0 mm in heavy rain as well as in windy conditions. When they compared each old and
125 new version of Parsivel with Joss-Waldvogel disdrometer and rain gauge measurements, the
126 new version of Parsivel (referred to as Parsivel^2 in their paper) appeared to have a noticeable
127 improvement over the old one for measuring drop size and rainfall rate.
128 To our knowledge, no studies of vertical air velocities retrieved from Parsivel-measured
129 drop size-fall velocity spectra have been documented or reported yet. In this study we utilize
130 Parsivel and anemometer data collected during intensive field observations that targeted to
131 investigate orographic rainfall mechanisms around mountain areas in the southern region of
132 Korea. A simple technique to retrieve vertical air velocities from Parsivel measurements is
133 developed and first applied to an orographic heavy rain event. This paper is organized as
134 follows. In Sect. 2, the retrieval technique and instruments used in this study are introduced.
135 A case description about the rain event is followed in Sect. 3. Results about characteristics of
136 up-/downward motion and related microphysics in the windward and leeward side are
137 presented in Sect. 4. A summary and conclusions follow in Sect. 5.
138

139 **2. Instrumentation and method**

140 Two main instruments used in this study are Parsivel disdrometer and ultrasonic

anemometer collocated at three different sites around Mt. Jiri (see Figure 1). Their data were collected during the intensive observation period from 13 June to 3 August 2016 to cover a summer rainy season which is called "Changma" in Korea were analyzed. Parsivel disdrometer (Parsivel), manufactured by OTT (Germany), uses laser-optical properties to measure both sizes and fall velocities of precipitation particles and derives quantities of radar reflectivity, precipitation intensity, etc from measured drop size spectra. Time resolution is 1 min. For more details about Parsivel, please see the Löffler-Mang and Joss (2000)'s paper. The ultrasonic anemometer (the Young Model 81000, hereafter UVW) measures east-west (u), north-south (v), and vertical (w) components of winds by using the speed of sound moving along winds between the three non-orthogonal sonic axes and generates wind speed and direction at 1-min interval. The accuracies are ±0.05 m s^{-1} for wind speed (0 to 30 m s^{-1}) and ±2 degrees for wind direction (0 to 30 m s^{-1}), respectively. The w component observed by UVW is referred to as w_{UVW}.

In this study, a simple, new scheme to derive vertical velocity (w) from Parsivel measurements is developed by using a relationship of Atlas et al. (1973) between terminal fall velocities and drop diameters in still air as shown by

$$V_f = 9.65\text{-}10.43*\exp(-0.6D), \quad (1)$$

where D is drop diameter (mm) and V_f is terminal fall velocity (m s^{-1}) and the vertical relation of air as shown below

$$w = V_p - V_f, \quad (2)$$

where V_p is Parsivel-measured fall velocity (m s^{-1}) averaged over 32 diameter x 32 velocity classes in a size and velocity spectrum. Altitudes of D1, D2, and D4 are 105, 280 and 313 m ASL, respectively. Due to the very low altitudes of these observation sites, change in atmospheric density with height is negligible and thus the atmospheric density correction

(Beard, 1985) on V_f is ignored. In all the terms, negative means downward. A mean w value at 1-min interval is finally estimated by subtracting V_p from V_f also averaged following the flowchart in Figure 2. The final w estimate is hereafter called w_{par}. For more details, please see the flowchart that shows how w is estimated from a 1-min drop size (D) and fall velocity (V_p) spectrum of Parsivel. Figure 3 illustrates three conditions of determining zero w, upward w, or downward w value for given D vs. V_p spectra. For the case 1, w would be zero since the D-V_p distribution closely follows the V_f line. Upward w value is determined for the case 2 that V_p is smaller than V_f (i.e., the distribution is towards below the V_f line). For the case 3, downward w value is determined since V_p is larger than V_f. For w_{par} validation, w_{par} is compared with w_{UVW} and its result is described in Sect. 4.

3. Case description

During a summer rainy season usually from late June to mid July in Korea, severe weather phenomena accompanied by heavy rainfall often occur in the southern region of the Korean Peninsula mostly covered by complex high mountains. In association with terrain-induced up-/downdrafts, mountainous areas can play an important role in controlling formation, amount, and distribution of rainfall. As precipitation systems move over these areas, they tend to develop rapidly and produce localized heavy rainfall. Observational analysis from radar and surface measurements in these areas is necessary to understand terrain effects on rainfall development and microphysics. Thus we performed intensive field observations around Mt. Jiri (1915 m ASL) in the southern Korean Peninsula during the 2016 summertime.

During the observation period of 13 June~3 August 2016, several rain events were observed. On 1 July 2016, a rainfall system associated with a Changma front has developed over the West Sea and moved towards Mt. Jiri. As it passes over the mountain from the east,

heavy rainfall was produced and observed by Parsivel disdrometers and UVWs from 1200 to 2200 LST. Figure 4 shows a distribution of accumulated rainfall on 1 July and the enlarged topography of Mt. Jiri with locations of observations. Large rainfall up to 90 mm was seen around the top and south of Mt. Jiri in relation to moist upwind flows in the windward side close to the ocean.

4. Results

4.1. w comparison in time series

For the w_{par} validation, the observed w_{UVW} is compared at time series. Time series of radar reflectivity (Z), rain rate (R), mass-weighted mean diameter (D_m) measured from Parsivel are also examined together. Three observation sites of D1, D2, and D4 where both the Parsivel and UVW data are available were selected out of total nine sites (Fig. 4b). D1 and D2 are windward and D4 is leeward of Mt. Jiri. Figure 5 shows the time series of Z, R, and D_m (top) and w (bottom) between the Parsivel and UVW observed at D1, D2, and D4. At D1 and D2, high $Z > 40$ dBZ and $R > 20$ mm h^{-1} are observed during the 1230-1330 LST period and at around 1730 LST in Figs. 5a and c. Correspondingly, large D_m values reaching 2 mm were analyzed in these periods. In Fig. 5e, high Z and R were also observed in the leeward side but showing a little time lag compared to those in Figs. 5a and c.

It is shown in Figs. 5b, d, and f that w_{par} matches quite well with w_{UVW}. On the windward side (D1, D2), they both show mostly upward motions and importantly, larger upward motions during periods of heavy rainfall (i.e., 1230-1330 LST and around 1730 LST). In contrast, downward motions are mostly observed on the leeward side (D4). It is noted in Fig. 5f that there existed a relatively large difference between w_{par} and w_{UVW} during these high R periods. We found that the difference is related to a decrease of V_p in these periods. For a given V_f, a mean V_p became smaller in Eq. (2) due to an increase of a larger number of small

drops ranged at 1~2 mm or a spread of small drops below the V_f line in the D-V_p distribution, more like the case 2 illustrated in Fig. 3. A physical reason for this is not clear yet but it is probably resulted from strong winds and turbulence during this high R periods. In other periods, they showed quite good agreement. Also, the maximum and minimum values of w_{par} and w_{UVW} hardly exceed ± 0.5 m^{-1}, almost one fifth of horizontal wind magnitudes (not shown), suggesting that winds are almost horizontal during the whole period and they point upward or downward slightly with the w signs. At D1 and D2, the relatively large w_{par} and w_{UVW} were found during heavy rain with $R > 20$ mm h^{-1} around 1300 and 1740 LST (Figs. 5b and d), indicating that updrafts contributed more on the substantial R increase on the windward side. In Fig. 5f, negative w_{UVW} values were found on the leeward side most of the time including the heavy rain period ($R > 20$ mm h^{-1}), suggesting that most of the rainfall on the leeward side occurred in more association with downward w motions.

Figure 6 shows characteristics of Z-R relations at D1, D2, and D4. Upward w_{par} values are colored in red and downward w_{par} in blue. They were changed to percentages by dividing by a total of counts in each class with $R > 0.5$ mm h^{-1}. At D1 and D2, the percentage for the upward w_{par} class is 61 % and 71 %, much larger than 39 % and 29 % for the downward w_{par} class, respectively. In contrast, the upward w_{par} percentage at D4 is 31 %, about a half or less than those at D1 and D2 as found in Fig. 5, and the downward w_{par} percentage is 69 %. Power-law Z-R relations in a form of $Z=\alpha R^{\beta}$ are compared between the observation sites in Fig. 6. There was a decrease in the coefficient α from D1 and D2 (250, 252) on the windward side to D4 (226) on the leeward side. The exponent β did not show notable change between the sides. The noticeable decrease in α suggests that for a given Z, R is larger at D4 than D1 and D2. This is consistent to histograms of DSD parameters in the later section showing the larger mean R and D_m at D4.

240 *4.2. Histogram analyses*

241 4.2.1 Characteristics of *w* histograms with regard to *R*

242 The w_{par} and w_{UVW} time series discussed in Sect. 4.1 are examined in their histograms of
243 frequency with regard to *R*. In this study, a simple *R* threshold, $R < 10$ mm h^{-1} and $R > 10$ mm
244 h^{-1} (Leary and Houze 1979; Testud et al., 2001), to discriminate stratiform and convective
245 rain was used although there have been a plenty of other methods based on DSDs and vertical
246 profiles to discriminate stratiform and convective rain (Bringi et al., 2003; Caracciolo et al.,
247 2006; Thompson et al., 2015; Thurai et al., 2016; Tokay and Short 1996; Tokay et al., 1999;
248 Ulbrich and Atlas 2002; Williams et al., 1995). Occurrences of upward and downward motion
249 were changed to percentage values as they are divided by a total count of upward and
250 downward *w* during the entire period. A bin size for these histograms is 0.05 m s^{-1}.

251 In Figs. 7a, b, c, on the whole, the w_{par} histograms are in good agreement with the w_{UVW} at
252 all three sites, showing the much better agreement in the stratiform class ($R < 10$ mm h^{-1})
253 than the convective class. The relatively larger difference between the w_{par} and w_{UVW}
254 histograms is found in the convective class of D1 and this is likely due to strong wind speeds
255 that tend to make a downward spread in measured *D* vs. V_p spectra of Parsivel.
256 Mathematically, this downward spread decreases Parsivel-measured drop fall velocities (i.e.,
257 decrease in V_p in Eq. (2)) and thus w_{par} becomes more positive, making a larger difference
258 with w_{UVW}. Compared to D4, the similar histograms of w_{par} are shown between D1 and D2.
259 That is, convective rain has occurred almost in association with upward motions, while for
260 stratiform rain, it occurred with both upward and downward motions (Figs, 7a and b). At D4,
261 in contrast, most of stratiform rain was associated with downward motions and convective
262 rain was associated with both upward and downward motions (Fig. 7c). Therefore, both
263 convective and stratiform rain was relatively more associated with downward motions on the
264 leeward side than on the windward side. Figures 7d,e,f show the areas occupied by the

upward and downward w motions in percentage at each site, same as those in the Z-R scatterplots shown in Fig. 6. The colored areas with the percentages show readily which w group is far dominant. As noted, upward motions were dominant at D1 and D2 while downward motions were dominant at D4. However, they did not show large percentage differences at all the sites, suggesting that either upward or downward motions have not happened overwhelmingly on each side in this event.

4.2.2 Characteristics of Z histograms with regard to w and R

The w_{par} properties discussed in Sect. 4.1 are examined by frequency histograms of Z with regard to w and R. In Fig. 8a, a much larger percentage (61 %) in the upward w group is found at D1 showing a relatively wider Z distribution, compared to that at D4 in Fig. 8d. In Fig. 8b, the R percentage classified as convective was 9 %, much smaller than 61 % in the upward w group in Fig. 8a, suggesting that 52 % of the upward w group was associated with stratiform rain. In order to study such relationships between w and R, histograms were split by four conditions in the upper-right corner shown in Figs. 8c and f. That is, each group of R > 10 mm h^{-1} and R < 10 mm h^{-1}, which is regarded as convective and stratiform rain, respectively, is separated by upward and downward w. Therefore, for instance, 91 % of the group R > 10 mm h^{-1} in Fig. 8c is equal to the sum of 52 % of the upward w and 39 % of the downward w group. Likewise, the upward and downward w group is also split by the two R conditions. Unlike D4 in Fig. 8f, there was no thick blue line at D1 in Fig. 8c because there were no data fell into this category of the downward w and R > 10 mm h^{-1} as shown in Fig. 7a.

In Fig. 8c, convective rain (R > 10 mm h^{-1}) with the largest mean Z has occurred solely in association with upward w motions (thick red line). Among the four categories, the majority percentage of 52 % was found in the category of the upward w and R < 10 mm h^{-1} at D1 but 65 % was found in the category of the downward w and R < 10 mm h^{-1} at D4. The widest Z

distribution were shown in these categories. In Fig. 8d, a much larger percentage is found in the downward *w* group as noted previously. In Fig. 8e, a larger percentage of 18 % is found in the group $R > 10$ mm h^{-1}, compared to the counterpart (9 %) at D1, indicating that on average sense, rain intensity was stronger at D4 (leeward). It is noted that at D4, convective rain has occurred in association with both upward (14 %) and downward motions (4 %) although the latter showed a bit smaller *Z* values than those in the upward *w*-convective rain category (thick red line). It is thus suggested that downward *w* motion can play a significant role in increasing *R*, even larger than 10 mm h^{-1} although the strongest *R* was related to upward motions rather than downward. Most of stratiform rain (< 10 mm h^{-1}) was associated with downward motions (65 %).

4.2.3. Histogram characteristics of DSD parameters with regard to w_{par}

In Fig. 9, we analyze histograms of DSD parameters that are obtained with additional *w* information from Parsivel, which is a first time ever, compared to conventional DSD studies. In this study, two histograms separated by the upward and downward *w* were obtained *per* each parameter. In Fig. 9b, The *Z* histograms at D4 show higher *Z* distributions with mean values of 34.8 and 25.6 dBZ in the upward and downward *w* category, respectively, are shown, compared to those (25.2 and 18.2 dBZ) at D1 in Fig. 9a. At both D1 and D4, the mean *Z*, *R*, and D_m values in the upward *w* category were higher than those in the downward *w* category. Between D1 and D4, the mean *Z*, *R*, and D_m over the entire data were higher at D4, indicating that rainfall intensity was somewhat stronger than D1 although the maximum *Z* (~50 dBZ) and *R* (near 60 mm h^{-1}) were quite similar each other (see the time series of *Z* and *R* in Fig. 5). The mean *R* of 15.1 mm h^{-1} was higher in the upward *w* category of D4 than 6.22 mm h^{-1} in that of D1 (Figs. 9c and g). The total mean *R* was 7.2 mm h^{-1} at D4, also larger than 4.3 mm h^{-1} at D1. The mean D_m was largest at 1.37 mm in the upward *w* category of D4 in

315 Fig. 9f and smallest at 0.86 mm in the downward *w* category of D1 in Fig. 9b. Thus, the mean
316 D_m (1.03 mm) in the downward *w* category of D4 was greater than that (0.86 mm) in that of
317 D1. This indicates that there were a comparatively larger number of large drops at D4 in
318 association with downward motions which were dominant during the entire period. Thus, it is
319 stressed that relative to the windward side, downward motions have more influenced the
320 growth in drop size and increase in *R* intensity in the leeward side.
321
322 **5. Summary and conclusions**
323 Intensive field observations for orographic rainfall around Mt. Jiri in the southern regions
324 of Korea were conducted during summertime in 2016. In order to examine up-/downward *w*
325 properties in the windward and leeward side of the mountain, a simple technique was newly
326 developed to retrieve vertical velocities (*w*) from drop size and fall velocity spectra of
327 Parsivel. Their comparison with the *w*-components observed by UVW showed quite good
328 agreement each other, producing the similar *w* histograms between the two instruments. On
329 the windward side (D1 and D2), upward motions were more frequently observed and
330 particularly larger upward motions were found during convective rain. For the leeward side
331 (D4), downward motions were more dominant even during the large *R* periods (> 10 mm h^{-1})
332 as in the windward side and most of stratiform rain was associated with downward motions.
333 Thus, it is speculated that downward motions have contributed more to drop growth and *R*
334 increase in the leeward side. It is important to note that as the rain system moves over the
335 mountain, upward and downward motions have occurred in the both sides of the mountain
336 although there existed differences in their frequencies of occurrence.
337 Eventually the newly developed technique that estimates *w* values from Parsivel drop size
338 and fall velocity spectra is found physically meaningful and promising although it needs to be
339 further tested in other places and events. It would be applicable to *w* retrieval and comparison

studies near the surface to investigate rain microphysics associated with up-/downward motion. The different properties of up-/downward motion in different locations stress their dependence on observed D-V_p distributions which vary largely as a result of complex factors such as rainfall intensity, up-/downdrafts, wind speed, turbulence, and so on.

In this study, both the observed and estimated w values were very small in magnitude mostly between -0.5 and +0.5 m s^{-1}, about one fifth of the measured horizontal wind speeds. As known, the w values are just a vertical component of winds. Thus the low w values indicate that winds blow almost horizontally and point up-/downward slightly with the w signs. During the high R periods, the estimated w values were larger in a positive sign (windward side), suggesting that there were more upward-pointing flows around the mountain. Probably this produces a large scale environment of converging-upward air and helps to intensify the orographic rain system, increasing Z and R.

The relatively large difference between w_{par} and w_{UVW} was found in the leeward side during the high R periods (Fig. 5f). This is probably associated with strong winds and turbulence that can spread the D-V_p distribution of drops down below the V_f line (particularly small drops) and further bias w magnitudes. Hence w retrievals using the disdrometer-based technique are not totally free from environmental conditions. Since the effects of winds and turbulence were not analyzed in this study, we will soon investigate their effects on D-V_p distributions and resultant w biases in a quantitative way as a subsequent work.

Acknowledgements

This research was supported by the National Strategic Project-Fine Particle of the National Research Foundation of Korea (NRF) funded by the Ministry of Science and ICT (MSIT), the Ministry of Environment (ME), and the Ministry of Health and Welfare (MOHW) (NRF-2017M3D8A1092021) and was supported by the New Faculty Start-Up Program funded by UNIST(Grant #: 1.160110.01).

390 **References**

391 Atlas, D., Srivastava, R. C., Sekhon, R. S., 1973. Doppler radar characteristics of
392 precipitation at vertical incidence. Rev. Geophys. Space Phys., 11, 1–35.
393 Atlas, D., Ulbrich, C. W., Marks, F. D., Black, R. A., Amitai, E., Willis, P. T., Samsury, C. E.,
394 2000. Partitioning tropical oceanic convective and stratiform rains by draft strength. J.
395 Geophys. Res., 105, 2259-2267.
396 Beard, K. V., 1985: Simple altitude adjustments to raindrop velocities for Doppler radar
397 analysis. J. Atmos. Oceanic Technol., 2, 468-471.
398 Bringi, V. N., Chandrasekar, V., Hubbert, J., Gorgucci, E., Randeu, W. L., Schoenhuber, M.,
399 2003. Raindrop size distribution in different climatic regimes from disdrometer and
400 dual-polarized radar analysis. J. Atmos. Sci. 60, 354–365.
401 Cao, Q., Zhang, G., Brandes, E., Schuur, T., Ryzhkov, A., Ikeda, K., 2008. Analysis of Video
402 Disdrometer and Polarimetric Radar Data to Characterize Rain Microphysics in
403 Oklahoma. J. Appl. Meteor. Climatol. 47, 2238–2255.
404 Caracciolo, C., Prodi, F., Battaglia, A., Porcu, F., 2006. Analysis of the moments and
405 parameters of a gamma DSD to infer precipitation properties: a convective stratiform
406 discrimination algorithm. Atmos. Res. 80, 165−186.
407 Cifelli, R., Williams, C. R., Rajopadhyaya, D. K., Avery, S. K., Gage, K. S., May, P. T., 2000.
408 Drop-size distribution characteristics in tropical mesoscale convective systems. J. Appl.
409 Meteor. 39, 760–777.
410 Friedrich, K., S. Higgins, F. J. Masters, and C. R. Lopez, 2013b: Articulating and stationary
411 Parsivel disdrometer measurements in conditions with strong winds and heavy rainfall. *J.*
412 *Atmos. Oceanic Technol.*, **30**, 2063–2080.
413 Jaffrain, J., and A. Berne, 2011: Experimental quantification of the sampling uncertainty
414 associated with measurements from PARSIVEL disdrometers. J. Hydrometeor., 12,

352–370.

Jameson AR, Kostinski AB. 1998. Fluctuation properties of precipitation. Part II: reconsideration of the meaning and measurement of raindrop size distributions. J. Atmos. Sci. 55: 283–294.

Kim, D.-K., and D.-I. Lee, 2016: Raindrop size distribution properties associated with vertical air motion in the stratiform region of a springtime rain event from 1290-MHz wind profiler, micro rain radar, and Parsivel disdrometer measurements, *Meteorological Applications*, 23, 40-49.

Leary, C. A., and R. A. Houze Jr., 1979: Melting and evaporation of hydrometeors in precipitation from the anvil clouds of deep tropical convection. J. Atmos. Sci., 36, 669–679.

Löffler-Mang, M., and J. Joss, 2000: An optical disdrometer for measuring size and velocity of hydrometeors. J. Atmos. Oceanic Technol., 17, 130–139.

Niu, S., X. Jia, J. Sang, X. Liu, C. Lu, and Y. Liu, 2010: Distributions of raindrop sizes and fall velocities in a semiarid plateau climate: Convective versus stratiform rains. *J. Appl. Meteor. Climatol.*, 49, 632–645.

Testud, J., S. Oury, P. Amayenc, and R. A. Black, 2001: The concept of “normalized” distributions to describe raindrop spectra: A tool for cloud physics and cloud remote sensing. J. Appl. Meteor., 40, 1118–1140.

Thompson, E. J., S. A. Rutledge, B. Dolan, and M. Thurai, 2015: Drop size distributions and radar observations of convective and stratiform rain over the equatorial Indian and west Pacific Oceans. *J. Atmos. Sci.*, **72**, 4091–4125.

Tokay, A., Short, D. A., 1996. Evidence from Tropical raindrop spectra of the origin of rain from stratiform versus convective clouds. J. Appl. Meteor. 35, 355–371.

Tokay, A., Short, D. A., Williams, C. R., Ecklund, W. L., Gage, K. S., 1999. Tropical rainfall

associated with convective and stratiform clouds: Intercomparison of disdrometer and profiler measurements. J. Appl. Meteor. 38, 302–320.

Tokay A, Hartmann P, Battaglia A, Gage KS, Clark WL, Williams CR. 2009. A field study of reflectivity and Z–R relations using vertically pointing radars and disdrometers. J. Atmos. Oceanic Technol. 26: 1120–1134.

Tokay, A., W. A. Petersen, P. Gatlin, and M. Wingo, 2013: Comparison of raindrop size distribution measurements by collocated disdrometers. *J. Atmos. Oceanic Technol.*, **30**, 1672–1690.

Tokay. A., Wolff, D. B., Petersen, W. A., 2014. Evaluation of the new version of the laser-optical disdrometer, OTT Parsivel^2. J. Atmos. Oceanic Technol. 31, 1276–1288.

Thurai, M., W. A. Petersen, A. Tokay, C. Schultz, and P. Gatlin, 2011: Drop size distribution comparisons between Parsivel and 2D video disdrometers. *Adv. Geosci.*, **30**, 3–9.

Thurai M, Bringi VN, Carey LD, Gatlin P, Schultz E, Petersen WA. 2012. Estimating the accuracy of polarimetric radar–based retrievals of drop-size distribution parameters and rain rate: an application of error variance separation using radar-derived spatial correlations. J. Hydrometeor. 13: 1066–1079.

Thurai, M., Gatlin, P. N., Bringi, V. N., 2016. Separating stratiform and convective rain types based on the drop size distribution characteristics using 2D video disdrometer data. Atmos. Res., 169, 416-423.

Ulbrich, C.W., 1992. Algorithms for determination of rainfall integral parameters using reflectivity factor and mean doppler fall speed at vertical incidence. J. Atmos. Ocean. Technol. 9, 120–128.

Ulbrich, C. W., and D. Atlas, 2002: On the separation of tropical convective and stratiform rains. J. Appl. Meteor. Climatol., 41, 188–195.

Williams, C. R., Ecklund, W. L., Gage. K. S., 1995. Classification of precipitating clouds in

the tropics using 915-MHz wind profilers. J. Atmos. Oceanic Technol., 12, 996-1012.

Williams, C. R., A. Kruger, K. S. Gage, A. Tokay, R. C. Cifelli, W. F. Krajewski, and C. Kummerow, 2000: Comparison of simultaneous rain drop size distributions estimated from two surface disdrometers and a UHF profiler. Geophys. Res. Lett., 27, 1763–1766.

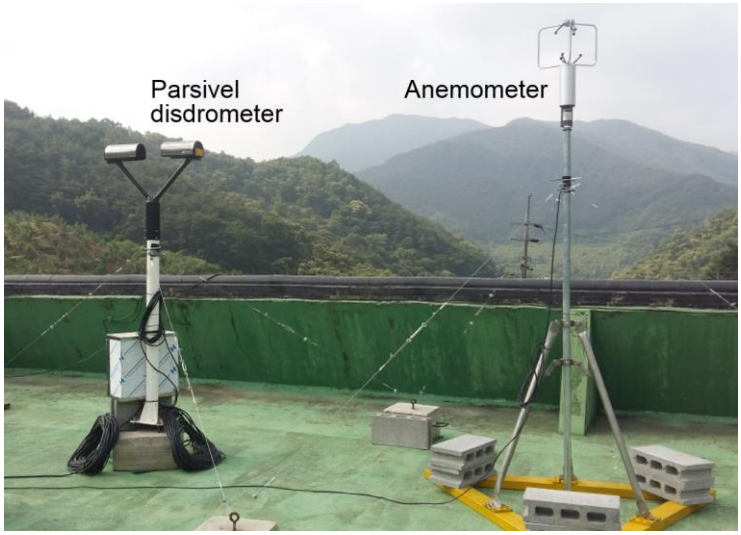

Figure 1. Picture of a Parsivel disdrometer and an ultrasonic anemometer that were installed at an observation site around Mt. Jiri during the intensive observation period.

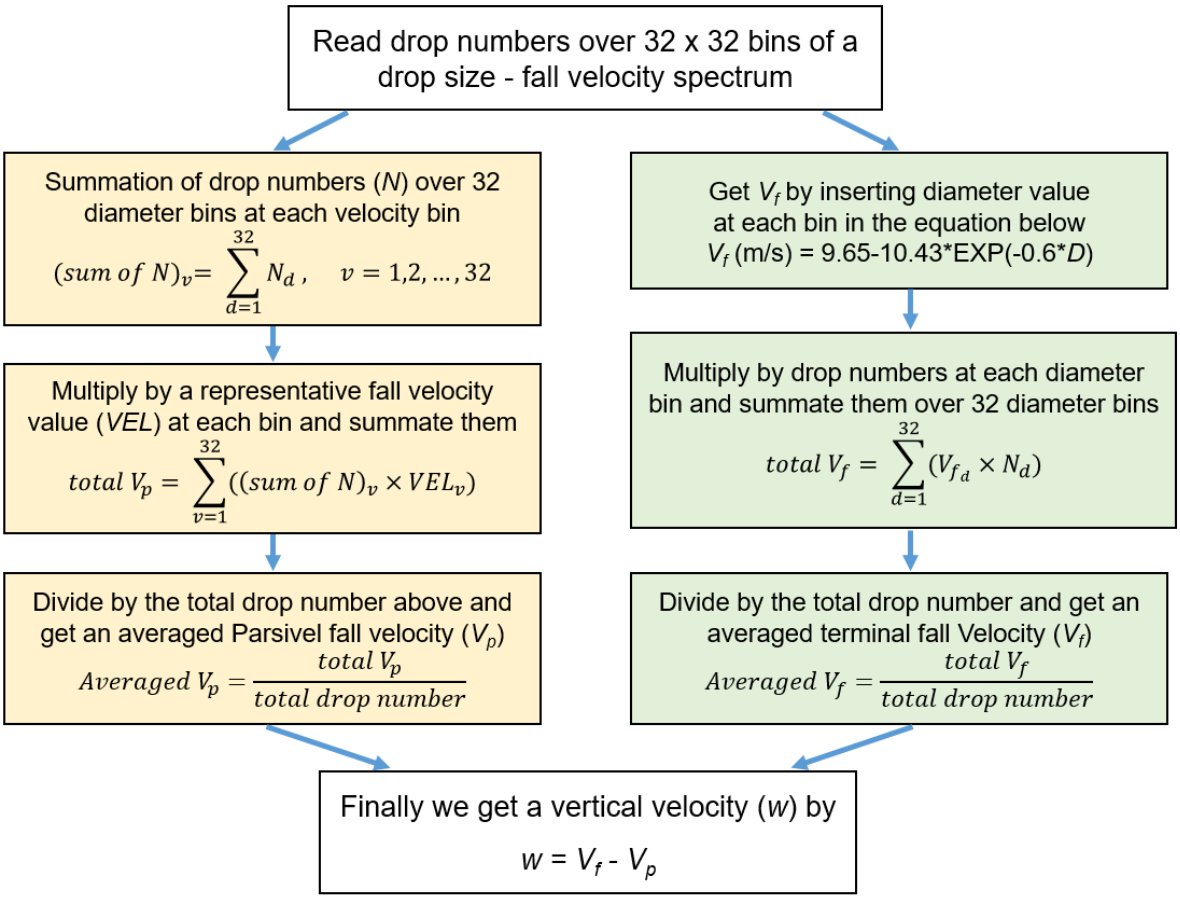

Figure 2. Flowchart for estimating w from a diameter-fall velocity spectrum of Parsivel (1-min interval). See text for more details.

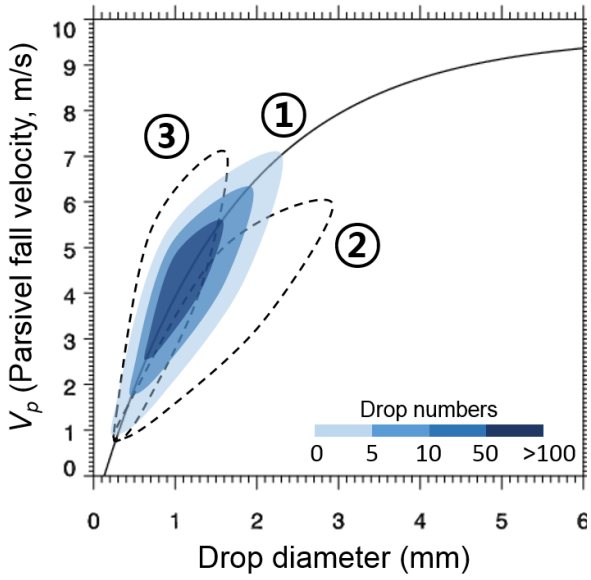

Figure 3. Schematic of Parsivel-measured diameter and fall velocity distributions for the three cases of determining zero *w*, upward *w*, and downward *w*. Solid line curve indicates terminal fall velocities (V_f) computed from Eq. (1). Contours show drop number concentrations. See text for more information.

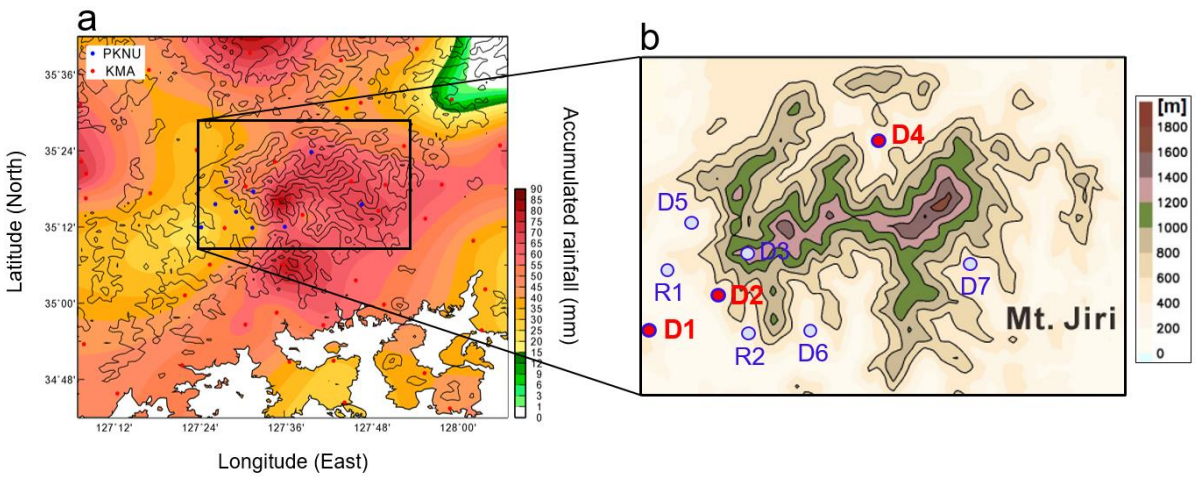

Figure 4. (a) Distribution of an acumulated rainfall (mm) on 1 July over contours of altitude at 300 m interval and (b) the enlarged topography of Mt. Jiri with contours of altitude at 200 m interval, showing nine observation sites. Three sites in red are where the Parsivel and UVW measurements were analyzed in this study. R1 and R2 show sites with a rain gauge only.

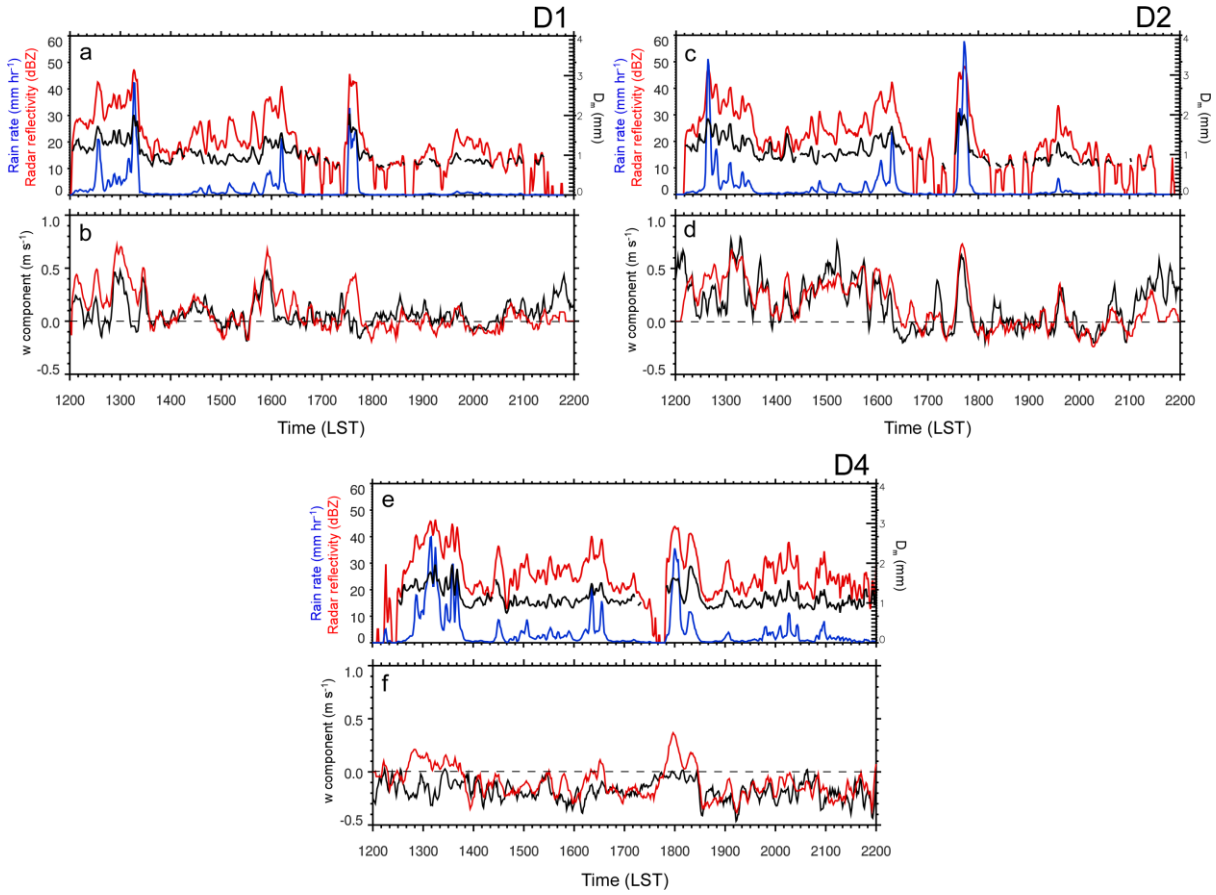

Figure 5. Time series of radar reflectivity (dBZ) in red line, rain rate (mm h^{-1}) in blue, and mass-weighted mean diameter (D_m, mm) in black at D1, D2, and D4 ((a),(c),(e)) and the time series of w_{par} (m s^{-1}) in red and w_{UVW} (m s^{-1}) in black at the same sites ((b),(d),(f)). LST stands for local standard time. 5-point running mean was applied.

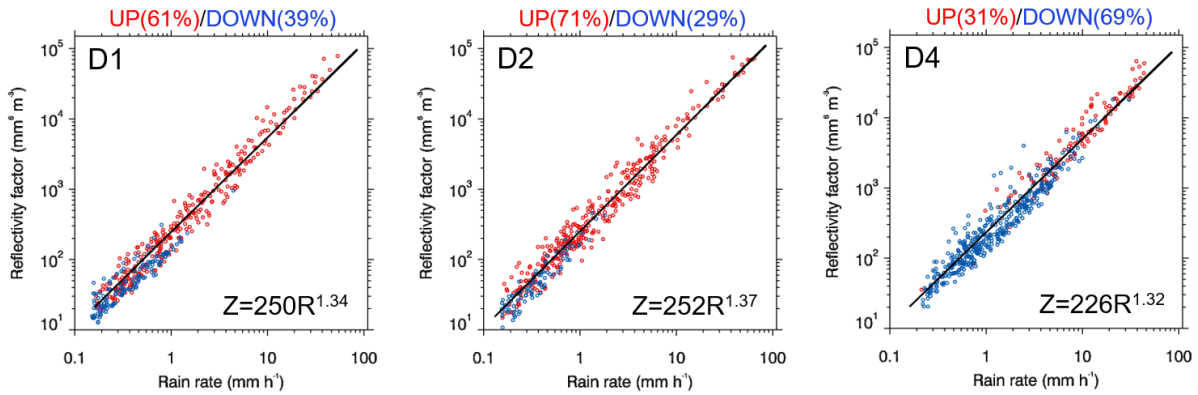

Figure 6. *Z-R* scatterplots at the three sites. Red dots indicate upward *w* and blue indicate downward *w*. Numbers on the top show percentages of frequency of occurrence in each *w* category.

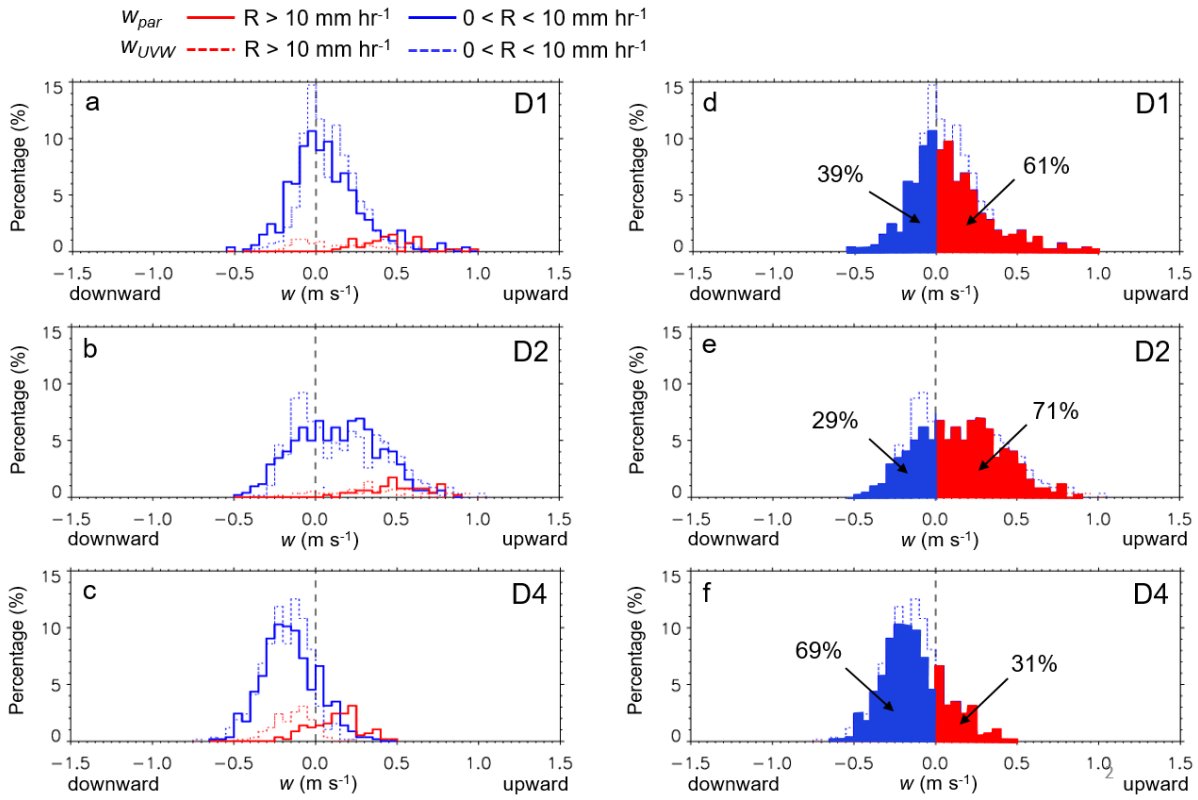

Figure 7. Frequency histograms of w (m s^{-1}) with regard to the two R groups (left panels) and those with percentages in the upward and downward w groups at the three sites (right panels).

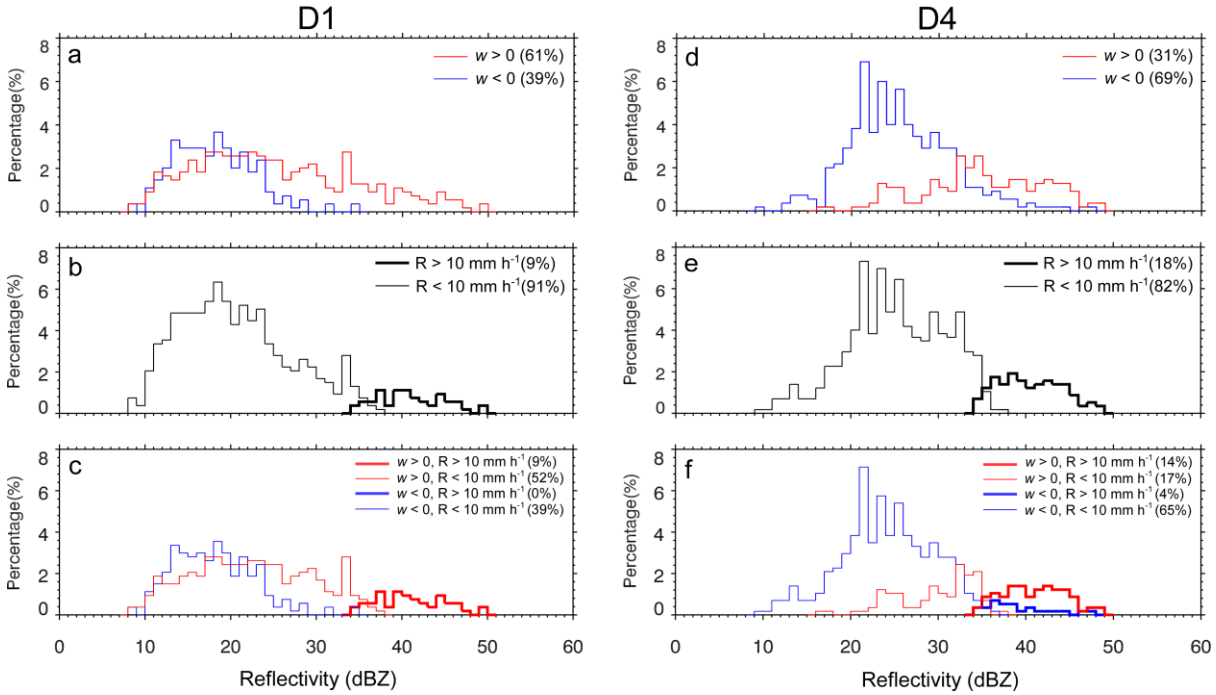

Figure 8. Frequency histograms of *Z* with regard to *w*, *R*, and these in the four groups with percentages at D1 and D4.

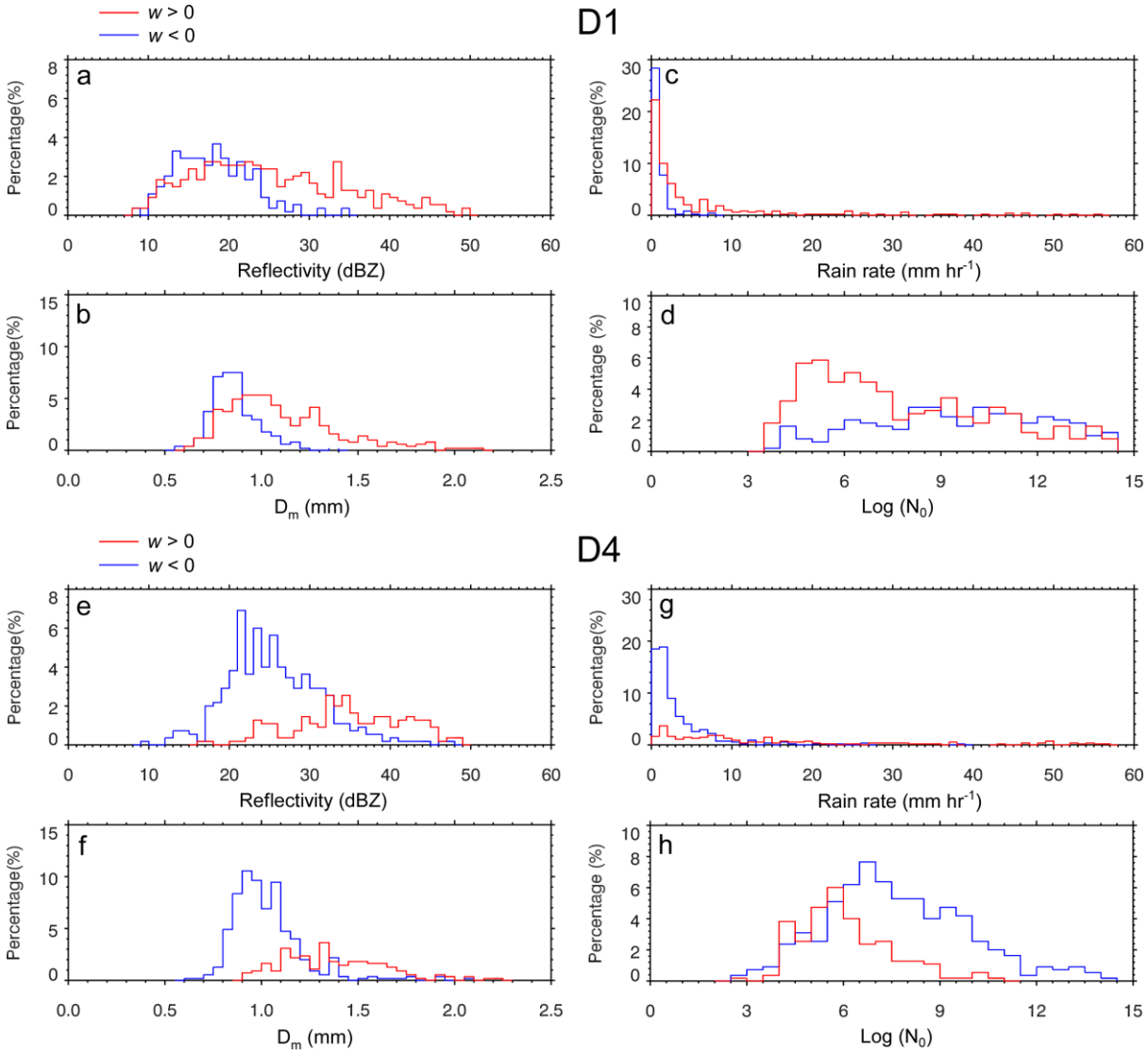

Figure 9. Frequency histograms of retrieved DSD parameters with regard to the upward (red line) and downward *w* (blue): (a) radar reflectivity (dBZ), (b) rain rate (mm h^{-1}), (c) D_m (mm) and (d) N_0 (m^{-3} $mm^{-1-\mu}$) in log scale at D1 (top four panels) and same as these but for D4 (bottom four panels).